minerals

MDPI

Article

Distribution Law of Mine Ground Pressure via a Microseismic Sensor System

Zilong Zhou [1], Yinghua Huang [1,2] and Congcong Zhao [1,*]

[1] School of Resources and Safety Engineering, Central South University, Changsha 410083, China
[2] State Key Laboratory of Safety Technology of Metal Mines, Changsha Institute of Mining Research Co., Ltd., Changsha 410012, China
* Correspondence: congcongzhao@csu.edu.cn

Abstract: The particularity of the occurrence conditions of the ore body in Xianglushan Tungsten Mine determines the mining form of the ore body and the particularity of the ground pressure distribution after mining. A large number of mined-out areas, supporting pillars, and natural and human factors have formed a comprehensive disaster environment. This can lead to frequent disasters, great harm, serious economic losses, and the necessity of severe environmental protection operations in the mine. This study aims to establish a microseismic monitoring system according to the actual needs of the site and to reveal the law of ground pressure manifestation by analyzing the distribution characteristics of microseismic events; to analyze the occurrence stability of the goaf; further verify it laterally; and finally, demonstrate the feasibility and effectiveness of the microseismic monitoring sensor system. In view of the current ground pressure problem in Xiangxuoshan tungsten mine, the stress change characteristics during dynamic mining and filling were obtained through comparative analysis of different perspectives such as surface change, energy release, and mining loudness, and key areas were identified to improve the reliability of underground ground pressure monitoring. The results show that the process of deposit destabilization caused by ore body mining can be further analyzed by microseismic monitoring, and the combination of surface settlement, mining intensity, and energy release can verify the accuracy of stress distribution and ground pressure transfer. In turn, the general reliability of underground ground pressure hazard warning is empirically improved.

Keywords: microseismic monitoring; ground pressure distribution; goaf; disaster; environmental protection

Citation: Zhou, Z.; Huang, Y.; Zhao, C. Distribution Law of Mine Ground Pressure via a Microseismic Sensor System. *Minerals* **2023**, *13*, 649. https://doi.org/10.3390/min13050649

Academic Editor: Mamadou Fall

Received: 13 April 2023
Revised: 5 May 2023
Accepted: 6 May 2023
Published: 8 May 2023

1. Introduction

The number of mined-out areas in mines around the world increases rapidly with the increase in mining scale, and the threat of mined-out area disasters is becoming increasingly serious [1–3]. In particular, there are many abandoned goaves in metal mines that constitute the main strategic reserve resources. With the extensive promotion of filling mining technology, disasters in goaves have been mitigated to a certain extent [4,5]. However, under the restrictions of technology and equipment available at the time, there are still mined-out areas with potential safety hazards that have not been properly solved [6]. In recent years, many scholars have proposed a variety of goaf ground pressure analysis methods, comprehensive disaster prevention, and early warning methods [7,8], which have achieved remarkable results in preventing goaf collapse and pillar instability [9] such as theoretical analysis [10], indoor acoustic emission test [11], numerical simulation [12], on-site microseismic monitoring [13,14], and on-site industrial test [15,16]. Marco et al. [17] argued that the goaf near the working face was the leading factor in the occurrence of disasters, which seriously threatens the safety of mine production. It mainly combines the microseismic monitoring technology and numerical simulation method to systematically analyze the stress distribution law of surrounding rock in the stope and reveal the precursor characteristics of ground pressure disasters in the adjacent working faces of the goaf.

Liu et al. [18] aimed to consider the occurrence of underground mine disasters from the perspective of informatization, automation, and intelligence. Future research should focus on intelligent microseismic data processing methods such as microseismic signal recognition and precise positioning algorithms, as well as the research and development of microseismic equipment.

Microseismic activities in underground mines related to mine pressure have been extensively studied [19]. In the mining process of underground mines, microseismic monitoring can reveal the performance characteristics of different types of damage in the form of repetition [20]. However, due to the characteristics of complex inducement, long activity cycles, and large randomness of ground pressure disasters in mined-out areas, many prevention and control methods of ground pressure disasters still cannot meet the needs of stability of mined-out areas caused by large-scale mining [21]. In general, the failure of goaves in underground mines is closely related to the stability of the roof, surrounding rock, and supporting pillars. From the perspective of stress distribution and transfer and disaster prevention, the internal structure and failure process of the surrounding rock and pillars should be the main focus [22,23]. The surrounding rock damage caused by mining changes its compressive strength, leading to roof collapse and pillar hand shear failure, and other accidents [24]. In recent years, microseismic monitoring technology has become increasingly mature in the stability monitoring and disaster prevention of rock mass structures [25–27]. The conventional approach of microseismic monitoring is to monitor the passive fracture source in real-time, online, and omnidirectionally [28,29]. There is a serious lag in the study of source location and mechanical characteristics of passive rupture sources through a microseismic monitoring system. This will lead to a lag in our research on disaster prediction. Therefore, we can understand the evolution law of the historical records of the existing data through the analysis of the existing data. In particular, it is a new comprehensive monitoring method combined with on-site filling and pillar protection measures. Combining the characteristics of microseismic monitoring technology and mining periodicity of ore and rock, we can understand and evaluate the breakage of surrounding rock and pillars through microseismic monitoring and analyze the weak areas of mechanical properties of the mine [30–33]. However, many studies do not seem to pay attention to the cooperative mechanism and evolution process of ground pressure redistribution and transfer via microseismic monitoring technology [34,35]. In this process, the lack of accurate control and effective guidance on the distribution of ground pressure [36] led to the occurrence of roof falls of surrounding rock and pillar instability [37], which can cause accidents.

Therefore, to study the interaction between goaf, surrounding rock mass, and pillar system in the mining process, we emphatically analyzed the characteristics and performance rules of ground pressure redistribution in the mining process based on microseismic monitoring data. At the same time, the ore yield, surface subsidence, and energy release parameters are used as verification analysis to protect the underground safety environment and surface geological environment of the mine. In addition, combined with the distribution of roof and floor, pillar, and microseismic events in the mining area, the space–time evolution law in the process of rock mass failure is revealed. Finally, this research provides a reference and basis for the stability analysis and research of large-scale and complex goaves.

2. Engineering Site and Microseismic Monitoring

2.1. Project Location Summary

Xianglushan Tungsten Mine is located in the northwest of Jiangxi Province, China (as shown in Figure 1a), and the surface morphology presented in Figure 1b shows that it has rich scheelite resource reserves (discovered in 1958 and put into production in 1991)—the second largest scheelite discovered in China [38]. The anticline structure of the mining area is gentle (as shown in Figure 1c), and the deposit is concealed [39,40] (as shown in Figure 1d). In addition, its shape is variable, and the rock strata are widely metamorphosed, resulting in large differences in the distribution of mine ground pressure [41–45].

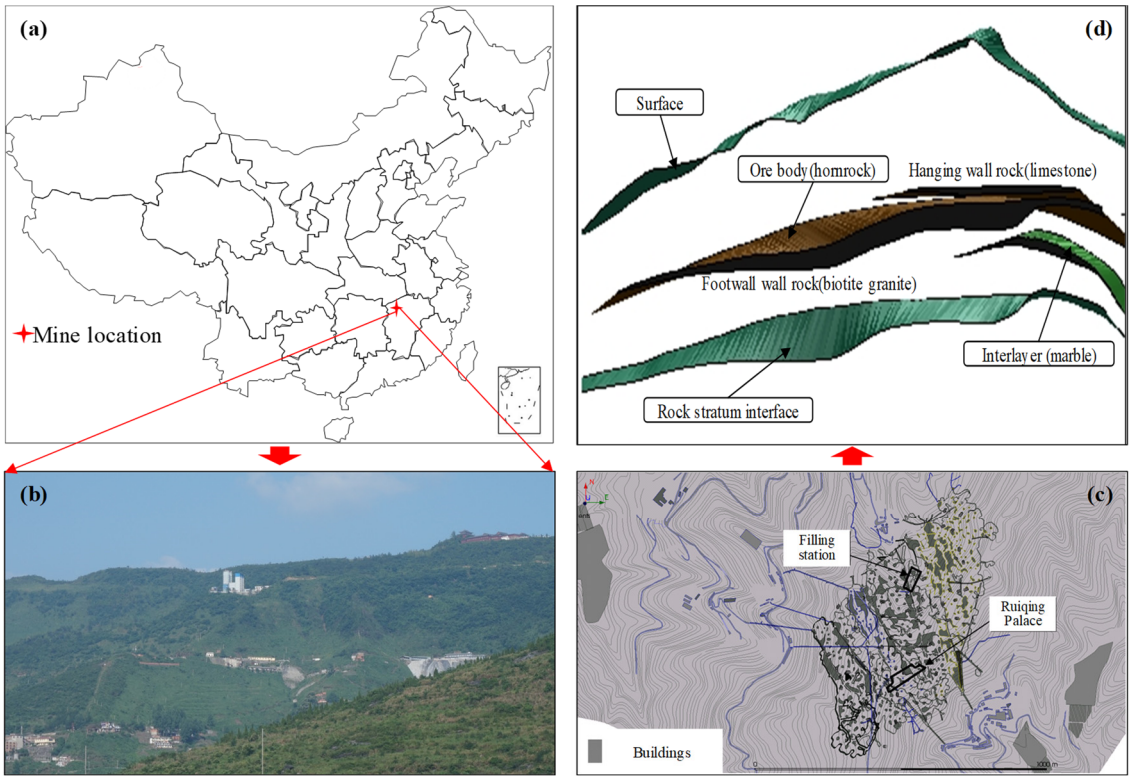

Figure 1. (**a**) Mine location. (**b**) Topographic and geomorphic map. (**c**) Overall drawing of goaf, surface, and important buildings. (**d**) Spatial distribution map of main rock strata.

Due to the influence of previous destructive mining and other historical mining reasons, the ground pressure in the goaf that causes phenomena such as pillar cracking, spalling, roof caving, and pillar and roof collapse is relatively serious. It can be seen that Xianglushan Tungsten Mine is facing a relatively serious problem with ground pressure safety production. This left a large number of potential production safety hazards for the follow-up mining and production of Xianglushan Tungsten Mine, and with the continuous increase in the mining area and goaf volume, the potential threat of large-scale ground pressure activities will also become greater and greater.

Since 2013, in the process of residual ore extraction in the Xianglushan Tungsten Mine, the geological environment and geological landform have faced severe challenges. Therefore, the project team began to study the safety and environmental protection between microseismic monitoring and mined-out areas. At this stage, ground pressure monitoring is mainly used to monitor and provide early warning of the overall ground pressure status of the mine, ensure the safety of production, and provide guidance for the treatment of the goaf.

2.2. Monitoring Network

To reproduce and analyze the law of ground pressure in the key areas of the mine, we built and optimized the microseismic monitoring system in Xianglushan Tungsten Mine. Figure 2 shows the layout of the main mining area and its microseismic monitoring system.

In terms of horizontal distribution, it mainly includes the eastern part (ellipse formed by blue dotted line) and the western part (ellipse formed by red dotted line). According to the occurrence characteristics and mining area of the ore body, it is divided into four areas with more detail. In the eastern region, magenta represents the main mining area between exploration lines 0# and 8#, yellow represents the main mining area between exploration lines 8# and 12#, and cyan represents the main mining area between exploration

lines 12# and 14#. In the western region, red represents the main mining area between exploration lines 14# and 18#.

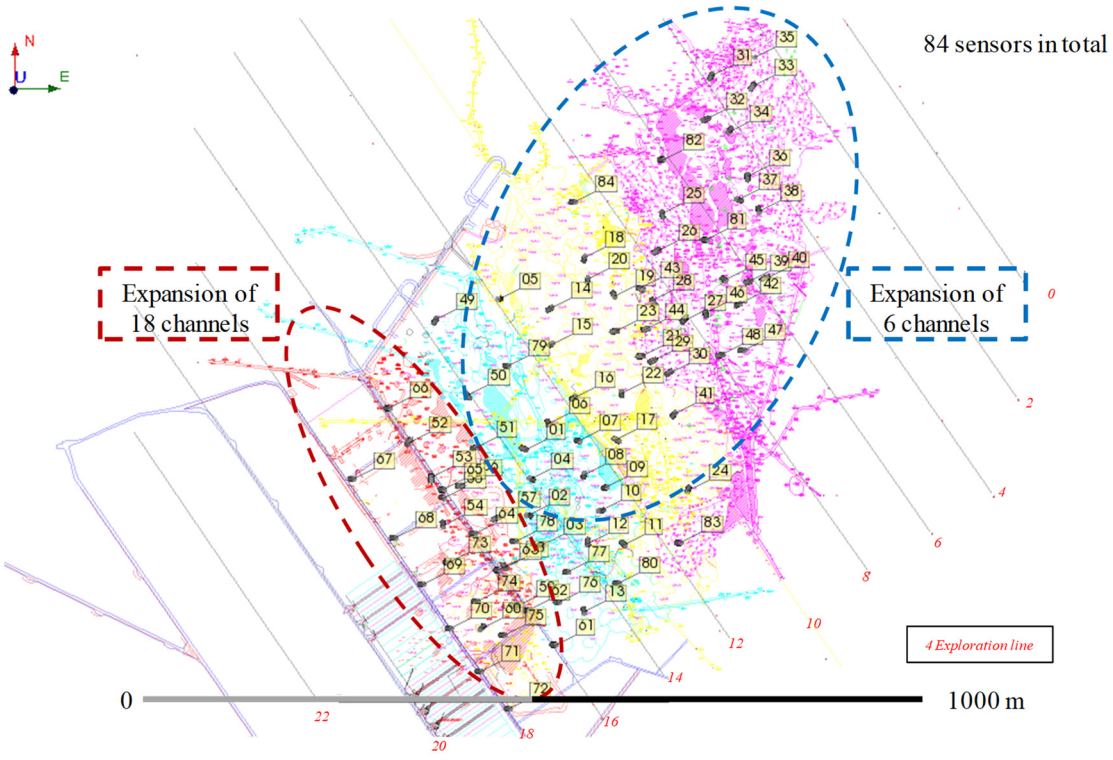

Figure 2. Plane distribution of microseismic monitoring sensor and exploration line position relationship.

According to the mining stage and scale, the east and west areas are divided by the 16# exploration line. A total of 24 new sensors are added. Eighteen sensors are distributed and installed between lines 16–18# in the west area. Six sensors are installed in the east of the 16-wire amplifier. Since the establishment of a 48-channel microseismic monitoring system underground in October 2010, a total of 4 years of uninterrupted monitoring had been carried out by September 2014. The total number of channels was expanded to 60 channels and 84 channels in September 2012 and September 2013, respectively, and the monitoring coverage was gradually expanded from the eastern residual mining area to the western mining area with 18~20 lines. The sensors in the east area mainly cover the pillars in the thick and large goaf. As shown in Figure 2, the cylinder is a sensor, numbered 1~84. There are 84 sensors in the expanded microseismic monitoring network.

The sensor used in Xianglushan Tungsten Mine is the original sensor equipped by the ESG Microseismic Monitoring System. All sensors in the system are single-axis acceleration sensors. The specific parameters are as follows: The sensor is a piezoelectric acceleration single-axis sensor. The sensitivity is 30 V/g, and the frequency response range is 50–5000 Hz. A data acquisition instrument simultaneously collects analog signals from six channels at a sampling rate of 20 KHz. The accuracy of converting analog signal to digital signal is 24 bits. Due to the need for microseismic event location, the microseismic monitoring system uses the time synchronization source generator of GPS timing, and the synchronization timing accuracy is 1×10^{-6} s.

Figure 3 presents the network topology of the microseismic monitoring system of Xianglushan Tungsten Mine. It shows the location and distribution of sensors in different zones. The topology is composed of sensors of signal acquisition hardware, Paladin of data acquisition and processing system, special cables of signal transmission and time synchronization system, software of integrated positioning and parameter calculation system, "brain" processing system of remote collaborative monitoring, and machine subsystem system of information transmission and network sharing system. All sensors were fixed in

the borehole by recyclable sensors to fully couple with the rock mass. Sensor cables were laid from underground to the surface through specific stopes and shafts. A new generation of high-precision multi-channel intelligent microseismic monitoring data analysis system for rock fracture developed by ESG company was installed in the ground control room. This intelligent monitoring system can effectively filter out environmental noise, which ensures that the data acquisition system and source positioning system operate accurately and normally. Microseismic data were recorded continuously at a sampling rate of 2000 Hz.

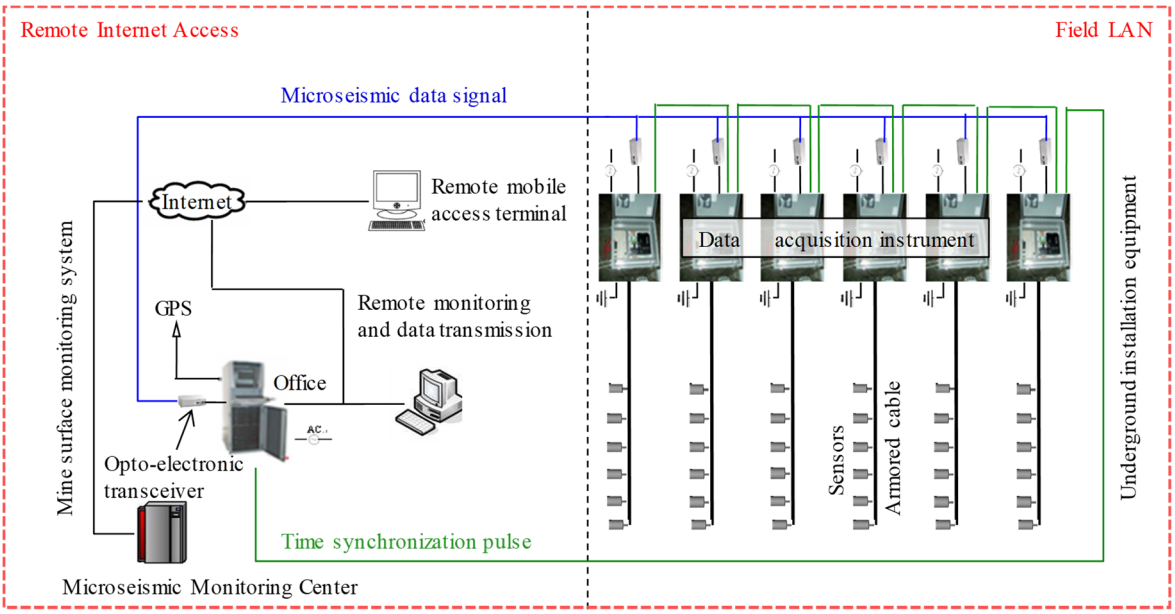

Figure 3. Network topology diagram of microseismic monitoring system in Xianglushan Tungsten Mine (Paladin expansion architecture diagram).

3. Analysis of the Distribution Law of the Overall Ground Pressure in the Mine

This paper mainly analyzes the microseismic monitoring data in the residual mining production process of Xianglushan Tungsten Mine in Jiangxi Province from October 2012 to September 2014. In addition, the microseismic monitoring data from October 2010 to September 2012 are also simply introduced as the basis for data analysis of the main interval. During the 48-month continuous monitoring period, there is a subtle relationship between the output scale of the residual ore body, the stress change of the surrounding rock pillar system, and the microseismic monitoring data, especially during the period from October 2012 to September 2014.

In the specific engineering environment of Xianglushan Tungsten Mine, the stress evolution of the surrounding rock–pillar-bearing system and the development state of the ground pressure activity can be well reflected by the microseismic data. The number, intensity, and temporal and spatial distribution of microseismic events can clearly and directly reflect the stress redistribution and concentration state of the surrounding rock–pillar-bearing system, as well as the laws and characteristics of ground pressure activities. This paper summarizes and analyzes the spatiotemporal distribution characteristics of microseismic positioning events from 2013 to 2018, reflects the evolution characteristics of the overall ground pressure distribution of the mine through the characteristics of microseismic activity, and discusses the relationship between microseismic activity and the stress in the mining process of residual ore bodies in order to guide mining and other activities.

In particular, on 28 June 2013, a large-scale roof collapse and ground pressure manifestation event occurred at the four pit mouths that intersected the eastern mining area and the western mining area. The large-scale goaf collapse event caused the overall stress transfer and redistribution of the mine, and it triggered the ground pressure manifestation event

of different scales in multiple areas. The following sections provide a detailed analysis and discussion.

3.1. Microseismic Monitoring Data Processing

In this study, we mainly obtained data for microseismic events that occurred in the study area from October 2012 to September 2014 for processing and analysis. During this period, a total of 103 effective microseismic positioning events were monitored and located underground.

Figure 4 shows the position relationship between the magnitude of the microseismic location event and the plane distribution. Figure 4 shows the magnitude and plane position distribution of the center of the earthquake, and the spherical shape represents the location and magnitude of the event. The color purple to red represents increasing magnitude, and the size of the spherical shape from small to large represents increasing magnitude.

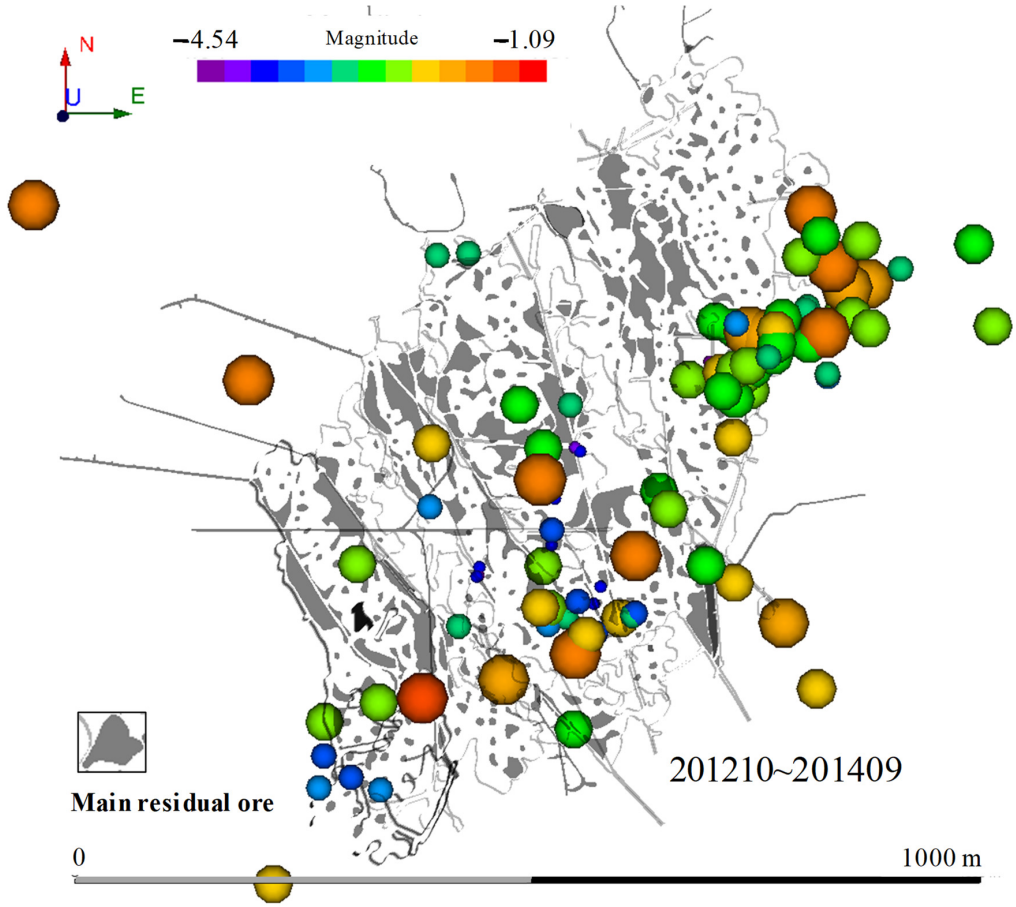

Figure 4. Spatial distribution of all microseismic positioning events that occurred underground from October 2012 to September 2014 (top view).

Figure 5a shows the relationship between the magnitude and time of the microseismic localization events. From the analysis, it can be seen that the magnitude range of microseismic localization event moments is between –2.0 and –0.2. Figure 5b shows the characteristics of the temporal distribution of all localization events within one day. From the analysis, it can be seen that the microseismic localization events are distributed at all hours of the day. There is a relative increase between 6:00 a.m. and 12:00 noon, which coincides with the actual production rhythm of the mine. Figure 5c shows the distribution of localization accuracy of microseismic localization events. In terms of the seismic source dimensional error, its main localization accuracy is between 10 and 20 m, with the largest number of events at 26. The positioning accuracy of less than 30 m reached 53 positioning

events, accounting for 51.5% of the total number of events. In general, the overall localization effect of microseismic localization events can match the depth of the research on this topic.

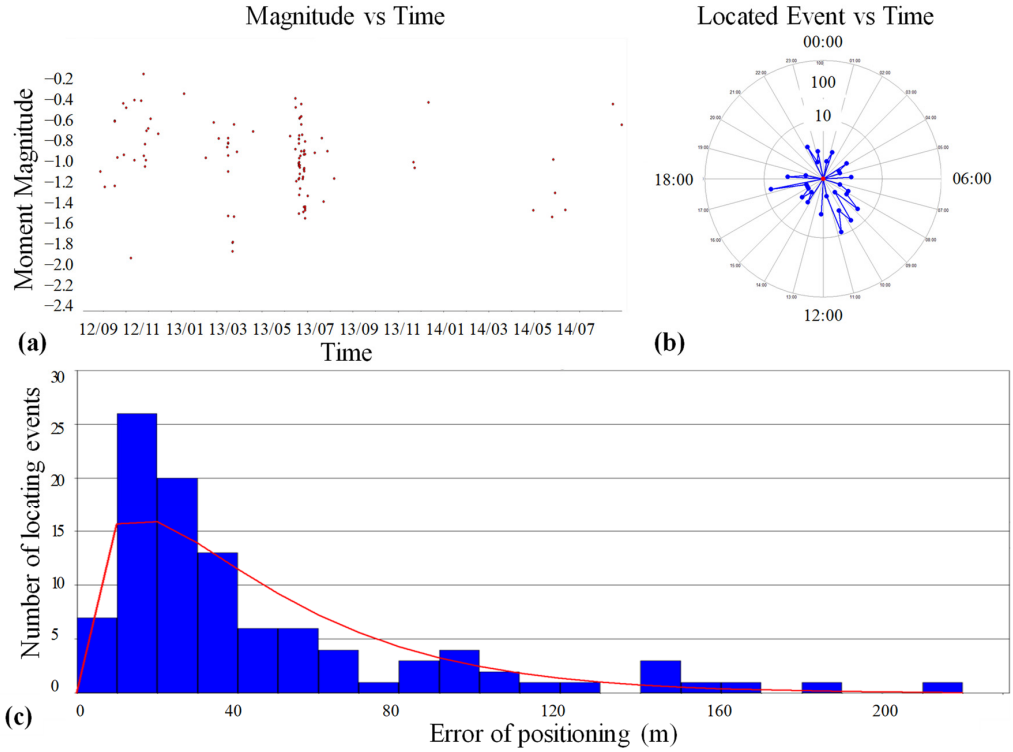

Figure 5. Characteristic distribution of microseismic monitoring events. (**a**) Time and magnitude. (**b**) NumA number of events at different times in a single day. (**c**) Location accuracy of microseismic events (X-axis: positioning error; Y-axis: number of events; Red line: corresponding percentage).

Figure 6 shows the development trend of the total number of single-channel events per day from October 2012 to September 2014, and shows the total underground pressure activity per day. Next, we will further analyze the relationship between mining intensity and underground ground pressure activities, and the dynamic development trend of underground ground pressure activities from 2012 to 2014. It can be seen from the analysis that the average number of single-channel events per day is about 50, and the average total relative energy is about 5000 mv. During the annual Spring Festival shutdown and overhaul holiday, the total daily microseismic activity level in the underground is much lower than the average level. For example, during the period from January 2013 to March 2013 and from November 2013 to March 2014, it is shown that underground ground pressure activity has a significant correlation with mining activities.

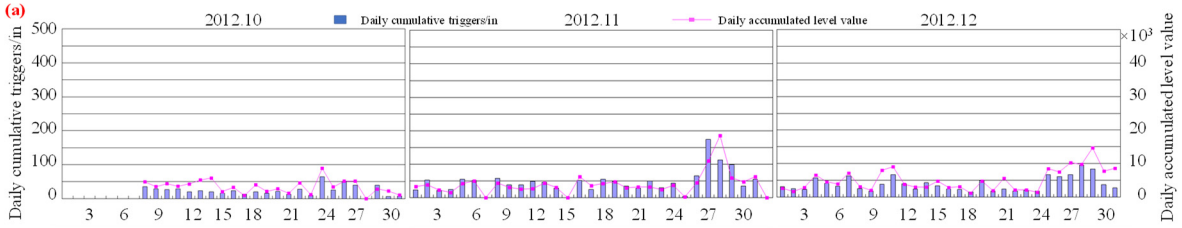

Figure 6. *Cont.*

Figure 6. Daily ground pressure trend chart in the study period (daily cumulative trigger events and daily cumulative level value). (**a**) October 2011–December 2011. (**b**) January 2012–December 2012. (**c**) January 2013–September 2013.

3.2. Analysis of Stress Concentration and Ground Pressure Transfer Characteristics

According to the microseismic characteristics of the damage at different locations of the mine site, the overall events are numerous and scattered in the overall monitoring range. If all dimensions are selected as the model boundary, the accuracy of local data analysis near the fault will be low. Next, we select the micro-earthquake events that can show the relationship between the occurrence of typical damage and micro-earthquake in the target period of Xianglushan Tungsten Mine for key analysis.

3.2.1. Distribution Law of the Concentrated Area of Microseismic Location Events

The microseismic positioning events monitored in the past two years are reproduced in the plane. As shown in Figure 7a, through observation and analysis, microseismic positioning events are mainly concentrated and distributed in the band area formed by two blue dotted lines in the figure. The strike of the strip area is the same as that of the ore body. In addition, the profiles of 6#, 12#, and 16# exploration lines are shown in Figure 7b–d, respectively. The location of microseismic location events is also delineated in the profiles of 6#, 12#, and 16# exploration lines. It can be seen that these positions are located at the place with the largest buried depth in the mined-out area, at the core of the "anticlinal" ore body, with a maximum buried depth of 200~300 m. The above microseismic monitoring data show that the microseismic positioning events in the mined-out areas with large burial depths are more concentrated than those in other areas.

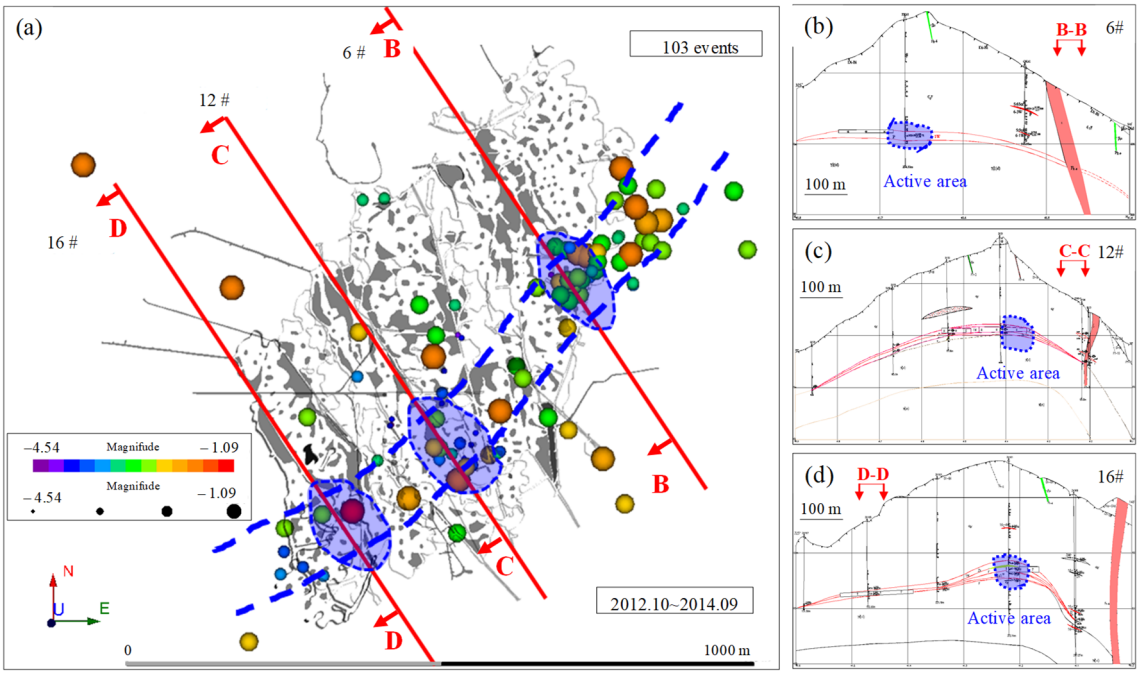

Figure 7. The relationship between the concentration bands of microseismic monitoring events and the profile positions of the main ground pressure manifestation points. ((**a**) Top view; (**b**) Section B-B; (**c**) C-C profile; (**d**) D-D profile).

It is reflected from the side that this type of damage is mainly caused by the buried depth. Therefore, it is preliminarily concluded that typical microseismic events are dominated by special damage category. Specifically, mine microseismic positioning events tend to be concentrated and distributed along the strike of the ore body, in the core of the "anticlinal" ore body, and the strip-type area with the largest burial depth. Figure 7a shows that the strip-type area along the strike of the ore body is the most concentrated place of the whole microseismic activity of the mine and the area with the highest concentration of stress. This strip area is the most likely place for future ground pressure activities and large-scale collapse of mined areas and is the key area for mine safety management.

3.2.2. Law of Stress Concentration and Transfer

From the perspective of mining disturbance stress transfer, it can be seen from the analysis of underground stress-monitoring results at the mine site, as shown in Figure 8, 2* measuring point has the largest increase in stress, and the increase in stress is about 1.1 Mpa. Moreover, 1* and 9* stress increase slightly, by 0.3 MPa and 0.34 MPa, respectively, and for 6*, the stress at the measuring point is unchanged and slightly decreased. The results of the stress meter measurement show that the stress in the fourth mining area in the west of the fifth pit mouth underground increased greatly. The stress in the 585 and 126 mining areas of No. 216 and No. 2 pit mouth is increased to a certain extent. The stress level of the 9* measuring point in the abovementioned measuring points gradually tends to be stable, and the trend of the stress level of 1* and 2* measuring points is still in a state of continuous increase on the whole. The stress in the mining areas of No. 4 and No. 216 and No. 585 and No. 126 in the west of No. 5 and No. 2 pit mouths is increased to a great extent, with the increase in stress ranging from 0.3 MPa to 1.1 MPa, and the trend is still in a state of continuous increase on the whole. By comparing the mining area with the stress concentration area, it can be seen that the mining disturbance in the mining area makes the stress in the surrounding area produce a certain degree of stress concentration. As shown in Figure 8, stress monitoring points are set at 2* and 1* positions. Around the remaining mining area, the stress changes of 2* and 1* sensors are 1.1 MPa and 0.3 MPa, respectively, that is, the new load on the pillar per unit area is 110 tons and 30 tons, respectively.

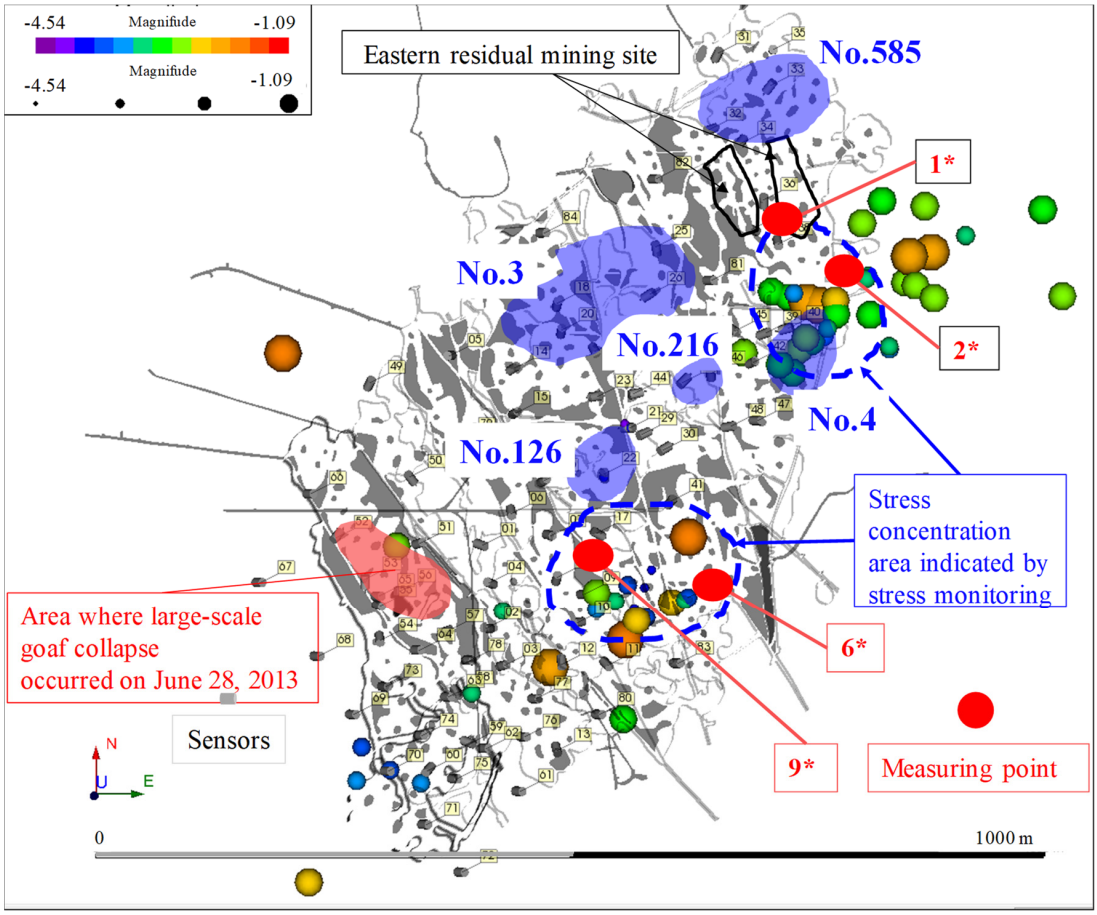

Figure 8. Regional distribution of stress transfer and concentration after large-scale collapse event.

In terms of the overall stress transfer of the mine, a comprehensive diagram of the underground microseismic monitoring and the location of the stress gauge from 28 June 2013 to September 2014 is shown in Figure 8, which shows the collapse of the large-scale mined-out area at the fourth pit mouth of the eastern residual mining area that occurred on

28 June 2013. It can be seen from the figure that the stress concentration areas reflected by the stress monitoring are consistent with the microseismic active areas reflected by the microseismic monitoring. This shows that there is great consistency between the active area of microseism and the area of stress concentration. After the production limit in the east of the two regions, small-scale collapse and other ground pressure phenomena continue to occur in local areas, indicating that the stress monitoring and microseismic monitoring have achieved good monitoring results, and the reflected underground ground pressure characteristics are consistent and reflect the actual situation.

According to the analysis of the gathering area of microseismic positioning events after the occurrence of large-scale mined-out area collapse, the microseismic positioning events are mainly distributed at the arch foot of the "anticlinal" ore body, indicating that the stress of the overlying strata after the large-scale collapse is transferred to and concentrated in the arch foot of the entire mined-out area's structural system. It shows that although the area with the highest concentration of underground stress is not at the arch foot at present, with the continuous occurrence of underground goaf collapse, the stress will mainly transfer to the arch foot. Therefore, the western mining area that adopts the room–pillar method for mining according to the design should be the key area for future ground pressure monitoring.

3.2.3. Distribution Law of Ground Pressure Manifestation Area

From October 2012 to September 2014, a total of 32 cases of ground pressure manifestation were counted through monitoring and warning cases of the microseismic monitoring system. These ground pressures show different scales, for example, large-scale collapse, local pillar cracking, and roof fall, on 28 June 2013.

As shown in Figure 9, the solid circle represents the position of each ground pressure display. The size of the circle indicates the scale of the relative ground pressure. The blue dotted line shows that the stability classification of goaf belongs to the scope of Class IV goaves of unsafe areas. Based on comparing the comprehensive map of the occurrence area of ground pressure manifestation with the distribution area of the Grade IV goaf, the overall law of the ground pressure manifestation area is as follows: most of the positions of ground pressure manifestation are within the range of a Grade IV stable goaf. The goaf with Grade IV stability is mainly characterized by a large roof span and small pillar size, which leads to the occurrence of roof fall and wall fragmentation in the goaf. Although these areas may not be those with the most concentrated stress, they are relatively susceptible to ground pressure safety accidents such as goaf collapse. Therefore, the goaf with Grade IV stability should be the key area for daily ground pressure safety management.

3.3. Analysis of the Influence of Microseismic Activity on Production Intensity

3.3.1. Relationship between Monthly Underground Ore Output and the Monthly Total Number of Single-Channel Events

Firstly, this is an approximate working condition comparison, which is an auxiliary pavement for the study of the ground pressure distribution pattern. The potential pattern of this type of event is reflected from different levels side by side. The underground ore yield was kept at 70,000~80,000 tons/month before the production limit in July 2013. After the production limit in the east, the ore yield was reduced to about 40,000 tons/month. Figure 10 shows the changing trend of monthly ore output from October 2010 to September 2014. At the same time, starting from the establishment of the microseismic system, the total number of single-channel events in the underground every month was counted, and its corresponding relationship with the monthly ore output is shown in Figure 11.

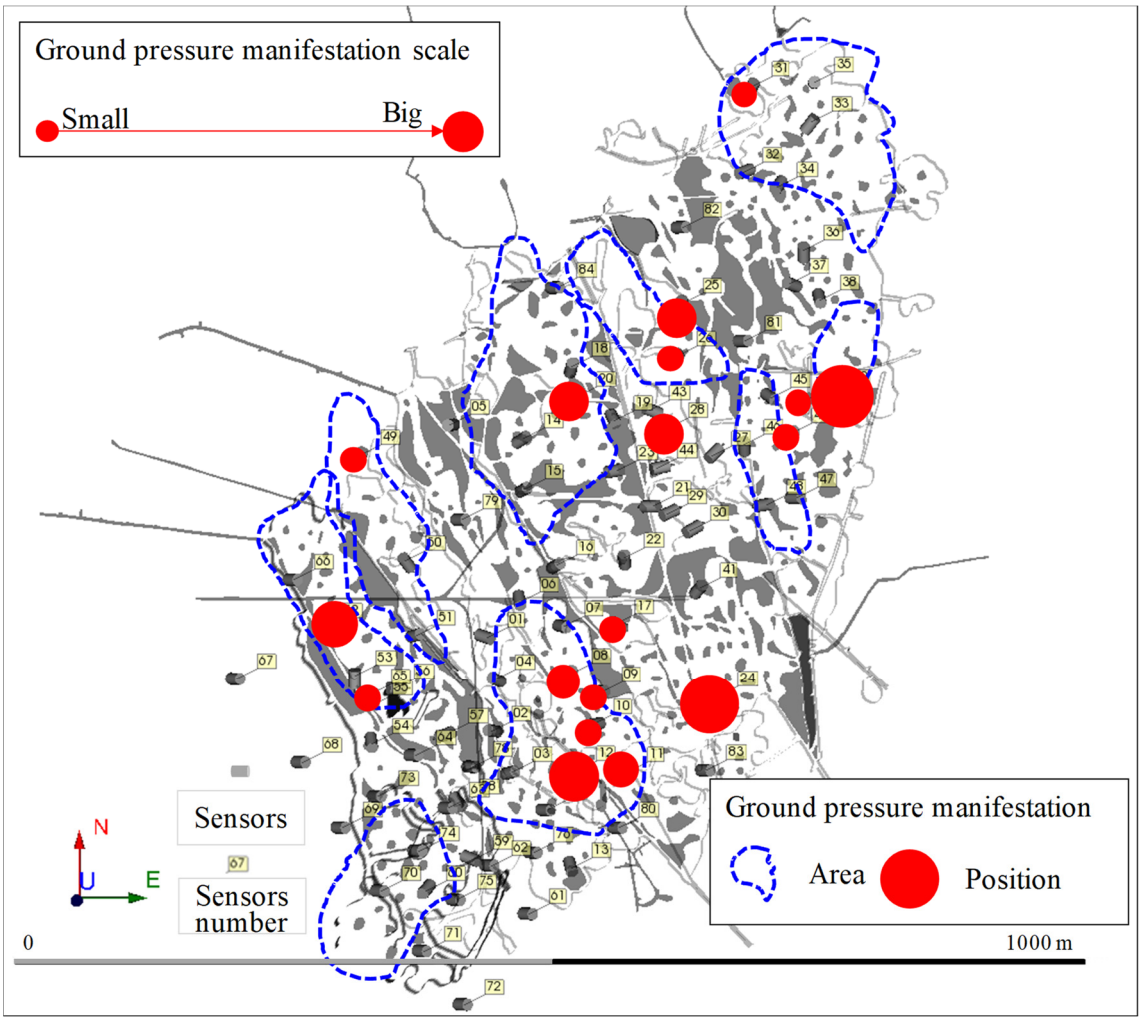

Figure 9. The relationship between the position distribution of ground pressure appearance and the area of Class IV goaf.

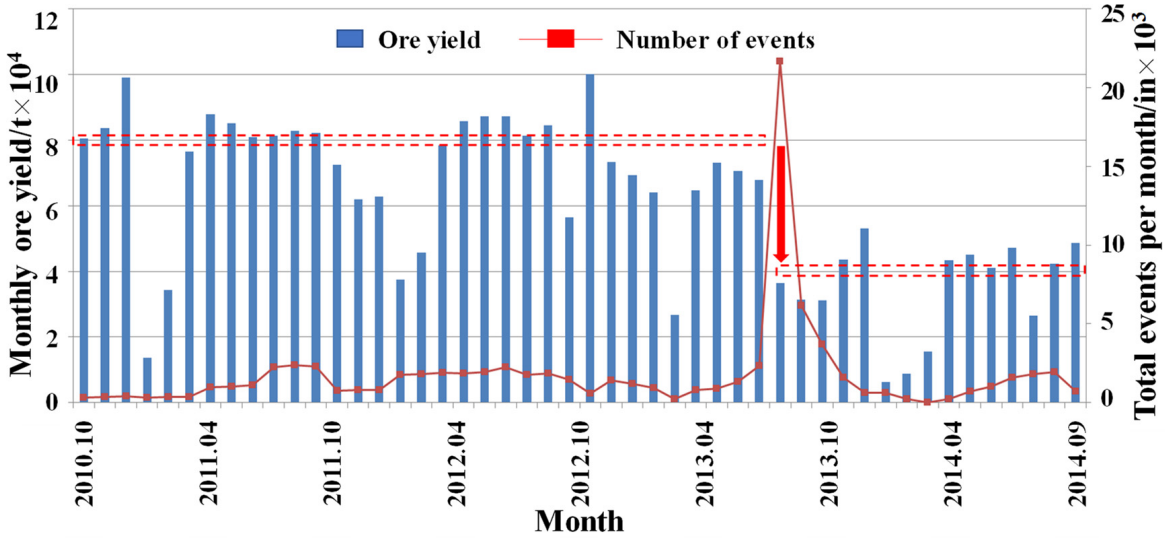

Figure 10. Trend chart of the relationship between monthly ore output and monthly single-channel events (October 2010~September 2014, 48 months).

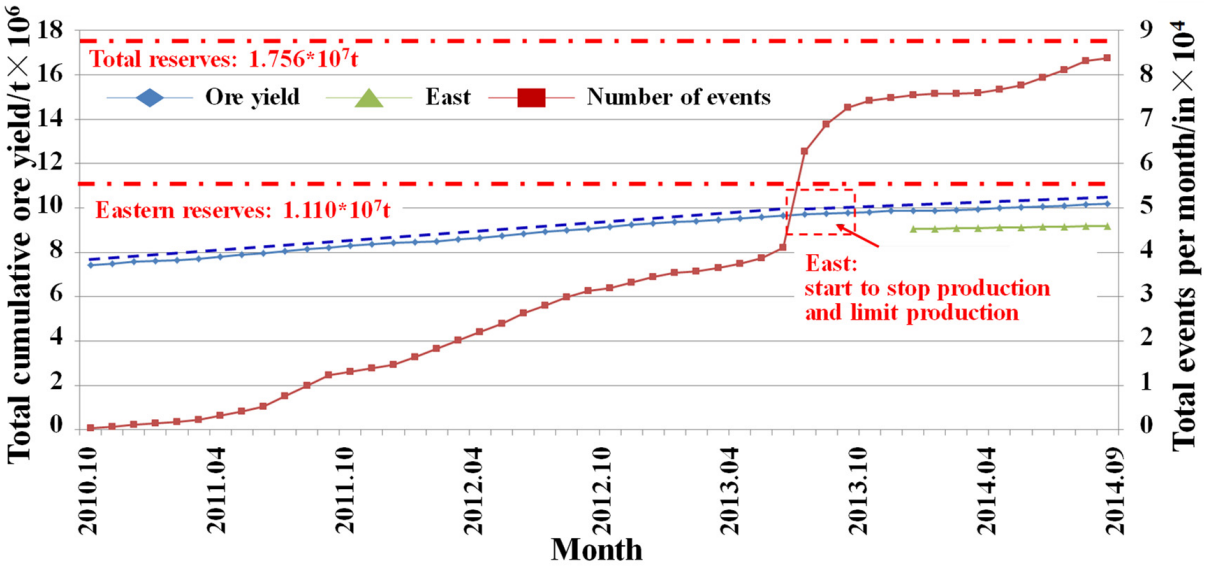

Figure 11. Trend chart of the relationship between cumulative ore yield and the cumulative total number of single-channel events. (October 2010~September 2014, 48 months).

During the period from October 2010 to May 2013, the total number of single-channel events per month was no more than 2500, ranging from 250 to 2400, with an average of about 1300. After the large-area roof collapse at the fourth pit mouth on 28 June 2013, the mine experienced the overall transfer and concentration of ground pressure, resulting in increased microseismic activity in several local areas and the occurrence of ground pressure. In July, August, and September after the production limit began in July 2013, the overall microseismic activity of the mine was still far higher than the historical maximum. The total number of single-channel events in July reached 21,669 and then decreased rapidly. However, the total number of single-channel events in September still reached 3717. The areas with a sharp increase in a microseismic activity mentioned above are mainly concentrated in the west fourth mining area, 216 mining area, north third mining area, and 585 mining area in the second mining area of the fifth mining area, and all have produced ground pressure manifestations of different scales. The above areas belong to the most unsafe Class IV area in the classification of goaf stability zoning. Since October 2013, the overall ground pressure transfer effect caused by the large-area roof collapse at the four pit openings has gradually slowed down. At the same time, the mining disturbance in the eastern mining area has been significantly reduced by limiting production, and the overall mine microseismic activity has gradually recovered to the level before the large-area collapse. The maximum number of single-channel events per month is not more than 2000, between 20 and 1951, with an average of about 1000.

The total reserves of the main ore body of Xianglushan Tungsten Mine are 17.56 million tons. By September 2014, 10.18 million tons had been recovered, of which the western part had been mined since September 2010, and about 1 million tons had been recovered by September 2014. The eastern part recovered about 9.18 million tons, while the total reserves of the eastern part of the ore body were 11.1 million tons, and the current recovery rate reached 82.7%. The trend chart of the relationship between the cumulative ore output of the eastern mining area and the cumulative total number of single-channel events is shown in Figure 11. Under the condition of the current high recovery rate in the east, the ground pressure situation faced by the next residual mining will be more serious, and the work of filling in the east, the study of stope ground pressure law, and the monitoring and warning of ground pressure disasters should be accelerated.

3.3.2. Relationship between Monthly Underground Ore Output and Total Monthly Positioning Events

From October 2012 to September 2014, 103 microseismic positioning events were monitored underground. The spatial distribution of microseismic events is presented in Figure 12a–c, which shows the spatial location of the location event during the period from October 2012 to 28 June 2013, from 28 June 2013 to 30 September 2013, and from October 2013 to September 2014.

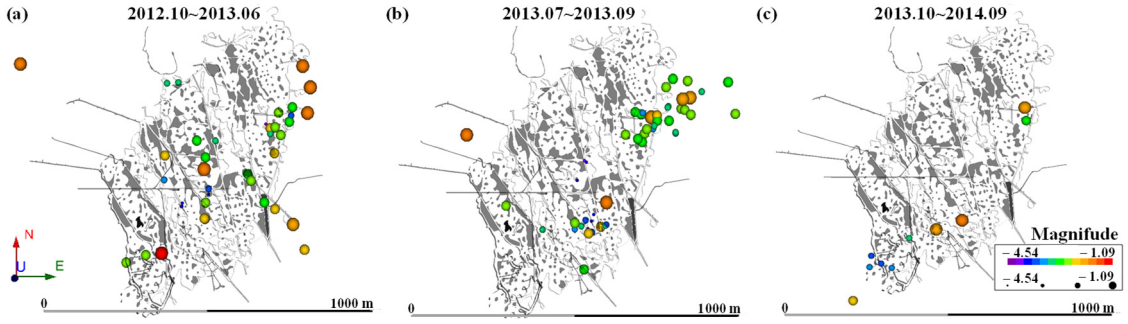

Figure 12. Spatial distribution of microseismic location events. (**a**) October 2012~June 2013. (**b**) July 2013~September 2013. (**c**) October 2013~September 2014.

Figure 13 shows that during the period from October 2012 to May 2013 the maximum number of events per month was not more than 12, ranging from 1 to 12, with an average of 5. On 28 June 2013, after the large-area roof collapse at the fourth pit mouth, the mine experienced an overall transfer and concentration of ground pressure, resulting in increased microseismic activity in several local areas and the occurrence of ground pressure. In the 3 months of June, July, and August after the start of the production limit in 2013, the overall microseismic activity of the mine was far higher than the historical maximum, with the total number of positioning events in June, July, and August reaching 20, 21, and 2, respectively.

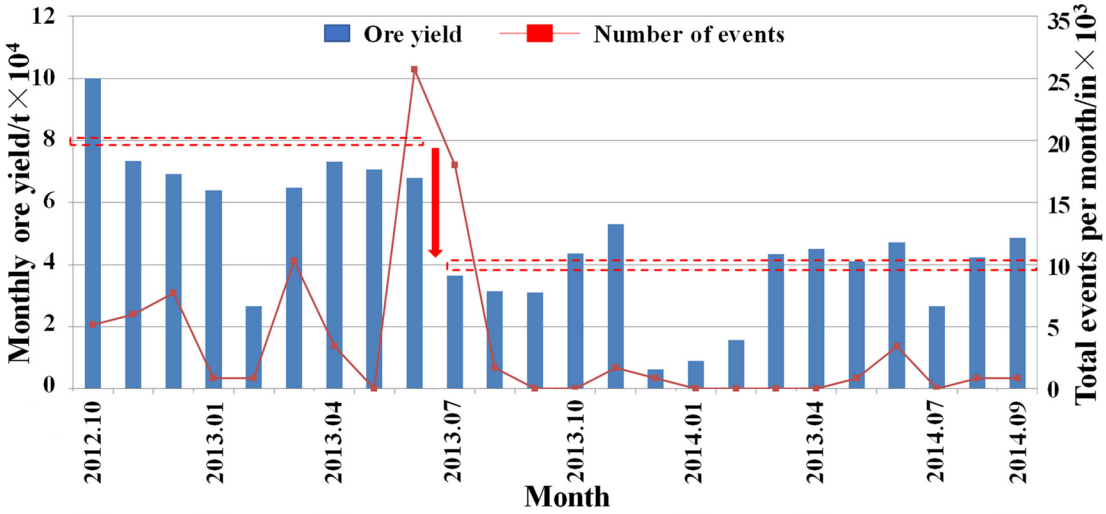

Figure 13. Trend chart of the relationship between monthly ore output and a monthly number of positioning events (October 2012~September 2014, 24 months).

The areas where the above microseismic activity has increased sharply are mainly concentrated in the west fourth mining area, 216 *, and 585 * in the second mining area of the fifth mining area, and all have produced ground pressure manifestations of different scales. It is also the most unsafe Grade IV area in the classification of goaf stability. Since September 2013, the overall ground pressure transfer effect caused by the large-area roof collapse event at the fourth pit mouth has gradually slowed down.

At the same time, the mining disturbance in the eastern mining area was significantly reduced by limiting production. The overall microseismic activity of the mine gradually recovered to the level before the large-scale collapse. In general, the ground pressure transfer and stress concentration show obvious consistency with the change in ore yield. Figure 14 shows the relationship between the cumulative ore yield and the cumulative total number of positioning events. Specifically, the total number of localized events per month is no more than 4, ranging from 0 to 4, with an average of about 0.8.

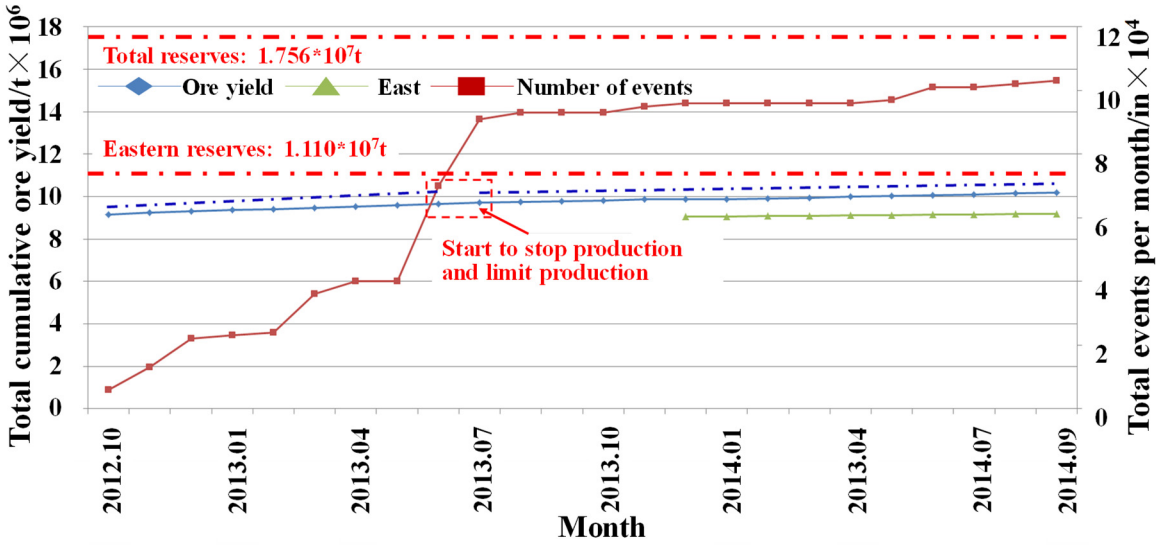

Figure 14. Trend chart of the relationship between cumulative ore yield and the cumulative total number of positioning events (October 2012~September 2014, 24 months).

3.4. External Performance Characteristics of the Overall Ground Pressure Development of the Mine

Through the above analysis, we know the characteristics of the distribution and transfer of mine stress and its production-related activity characteristics during the analysis period. In addition, the overall data are consistent by year, and they do show obvious changes. The spatial distribution and evolution of microseismic positioning events monitored underground from 2013 to 2018 are shown in Figure 15. In terms of the overall evolution, it shows the specific location, magnitude, and aggregated location and magnitude information of microseismic positioning events each year. It also shows how to verify it by other auxiliary methods, and then verify the relationship between ground pressure and microseismic events by parameters such as surface subsidence and energy release.

3.4.1. Analysis of Development Characteristics of Ground Pressure Based on Surface Subsidence

Through the survey point layout and data monitoring and analysis of specific underground points, we can see that the deformation of all survey points on the surface is not obvious in all directions except for the accumulated deformation of 20 mm in the due north direction of 1 * survey point (the horizontal survey accuracy is 10 mm). However, there are large fluctuation anomalies. Figure 16 shows the development trend of total settlement in the elevation direction of each measuring point on the surface. It can be seen that the surface settlement deformation is not obvious and has not caused a major hard impact temporarily. Continuous observation should be maintained to assess its future development trend.

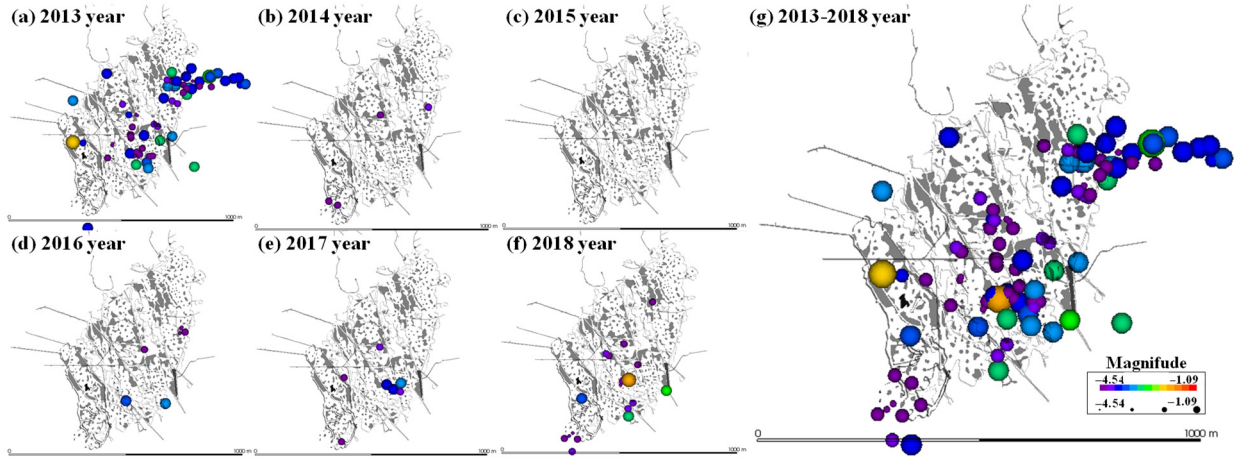

Figure 15. Evolution diagram of space–time distribution of underground microseismic positioning events.

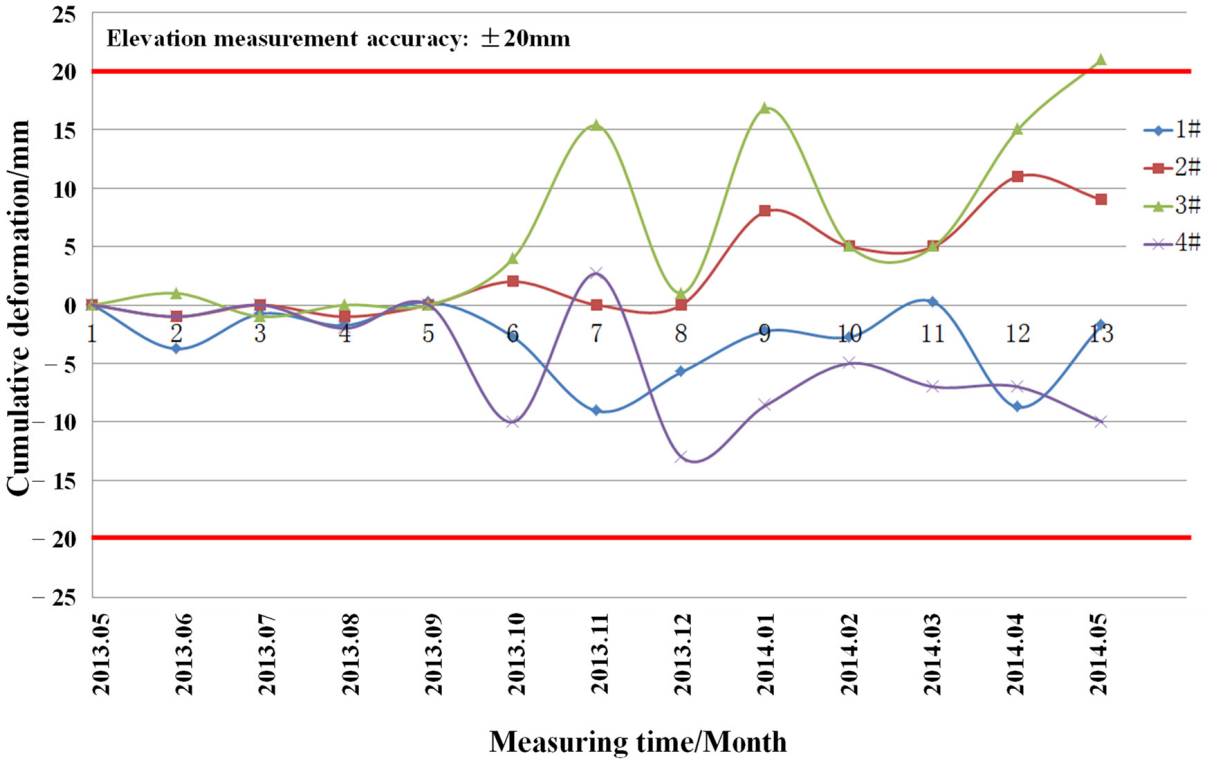

Figure 16. Development trend of total settlement at each measuring point on the surface (May 2013~May 2014).

Figure 17 shows the development of underground pressure appearance times before and after the large-area collapse. It can be seen that the number of ground pressure manifestations peaked in July and August after the large-scale collapse event on 28 June 2013, which was greater than the historically highest level before the large-scale collapse event, indicating that the underground stress redistribution and concentration after the large-scale goaf collapse event entered a peak period. With the end of the stress adjustment period of three months after the large-scale goaf collapse event, the number of ground pressure manifestation events is again at the average level before the large-scale collapse.

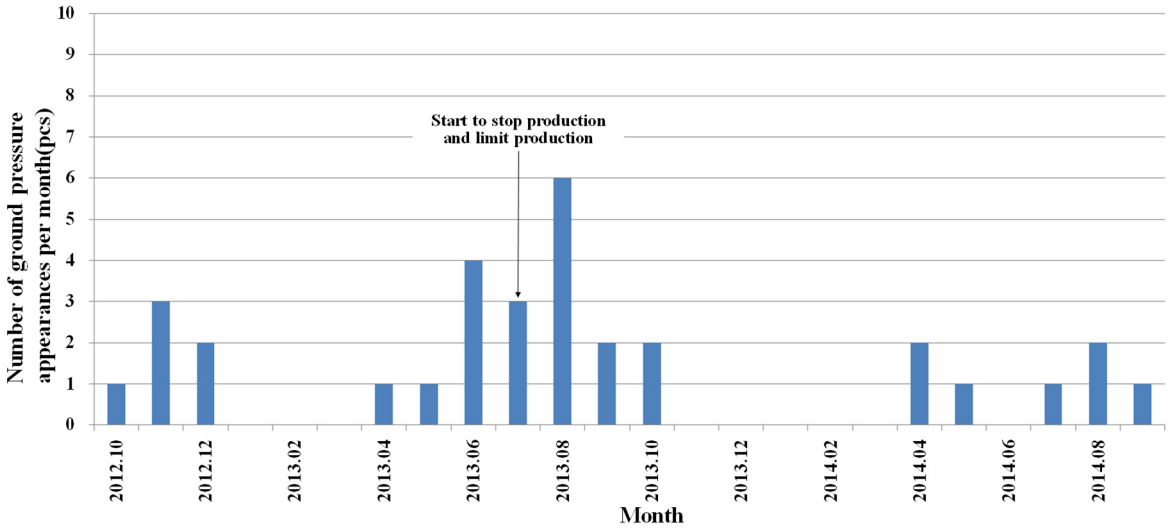

Figure 17. Change the trend of ground pressure before and after large-area collapse.

3.4.2. Analysis of the Development Characteristics of Ground Pressure Based on Energy Release

From Figure 15, it can be seen that the spatial distribution and evolution process of microseismic positioning events were monitored underground from 2013 to 2018. The figure shows in detail the specific location and magnitude of microseismic positioning events for each year. Combined with the change of the whole process, we analyzed the change law of microseismic events and their energy release to reflect the characteristics of ground pressure change from the side and verify them. The annual event rate and cumulative energy release rate of underground microseismic positioning are shown in Figure 18.

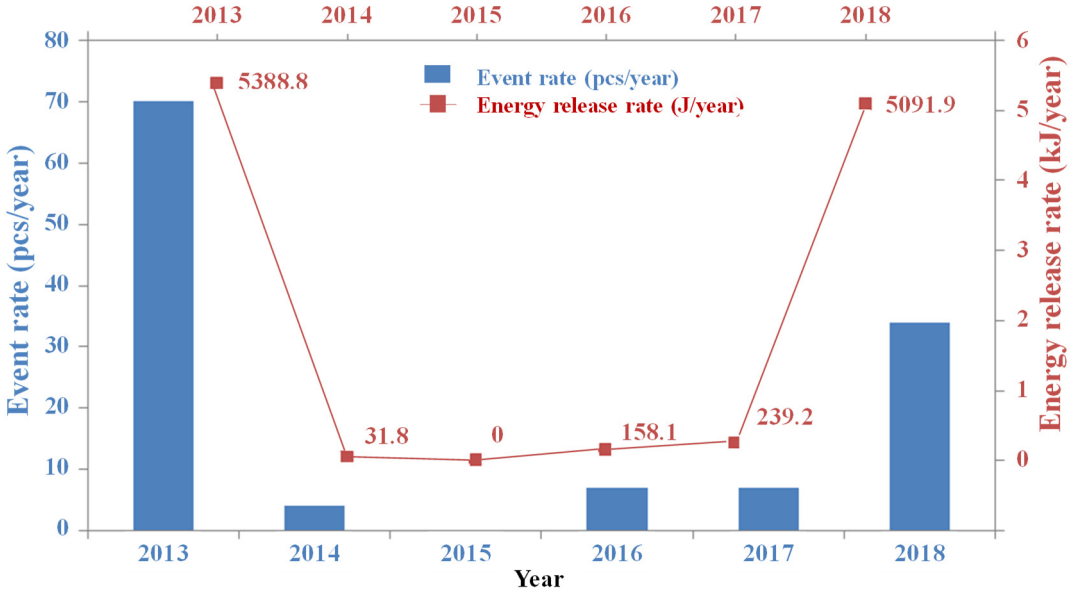

Figure 18. Trend chart of downhole microseismic positioning event rate and cumulative energy release rate per year.

A total of 122 microseismic positioning events were monitored from 2013 to 2018. The most active microseismic positioning events in 2013 totaled 70. After the production of the eastern residual mining area began to decrease in the second half of 2013, the microseismic positioning events decreased significantly in the four years from 2014 to 2017. The number

of microseismic positioning events per year is only 0–7, lower than the level of 10% in 2013, and the microseismic activity rate is significantly reduced. At the same time, the frequency and intensity of underground ground pressure are also in a corresponding state of relaxation, and the ground pressure situation is slowing down. However, in 2018, the number of microseismic positioning events increased to 34, and the cumulative energy release rate was similar to that in 2013. In 2013, it was 5388 J, and in 2018, it was 5091 J, which indicates that the underground microseismic activity rate in 2018 had started to intensify again. At the same time, the frequency and intensity of underground ground pressure manifestation increased significantly. It indicates that the underground pressure situation in 2018 will start to deteriorate again.

According to the above analysis, underground microseismic activity in 2018 increased significantly compared with that in 2014–2017. The spatial distribution of underground microseismic positioning events in 2018 is shown in Figure 19. It can be seen that 34 microseismic positioning events are distributed in and near the core of the "anticlinal type" with the largest burial depth. This shows that after the development and transfer of large ground pressure in the early stage, the energy release is much slower and there is essentially no obvious concentration phenomenon in the location. It also shows that the law of ground pressure development and transfer can be objectively verified by microseismic monitoring data.

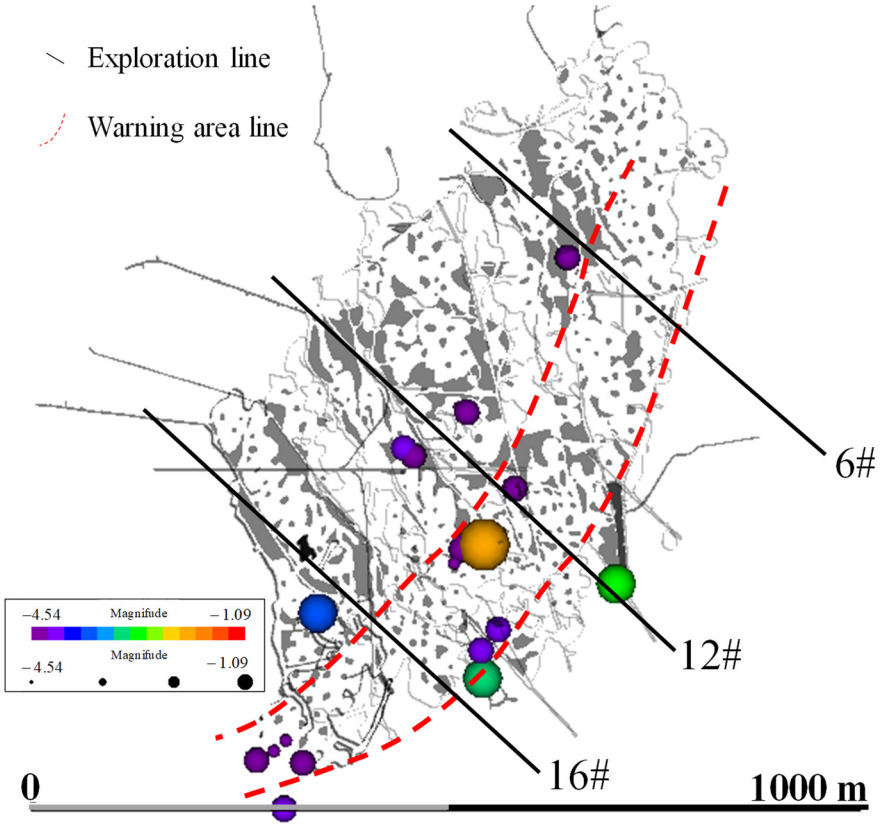

Figure 19. Spatial distribution of underground microseismic positioning events in 2018.

With the release of energy, the characteristics of moment magnitude change of microseismic events reflect the magnitude and indicate the degree of damage. It can reflect the fracture area, average dislocation momentum, and shear modulus of rock at the dislocation of microseismic events. The changing trend of the moment magnitude of microseismic positioning events with time in 2018 is presented in Figure 20, which shows that, in October 2018, the maximum moment magnitude reached 0.3.

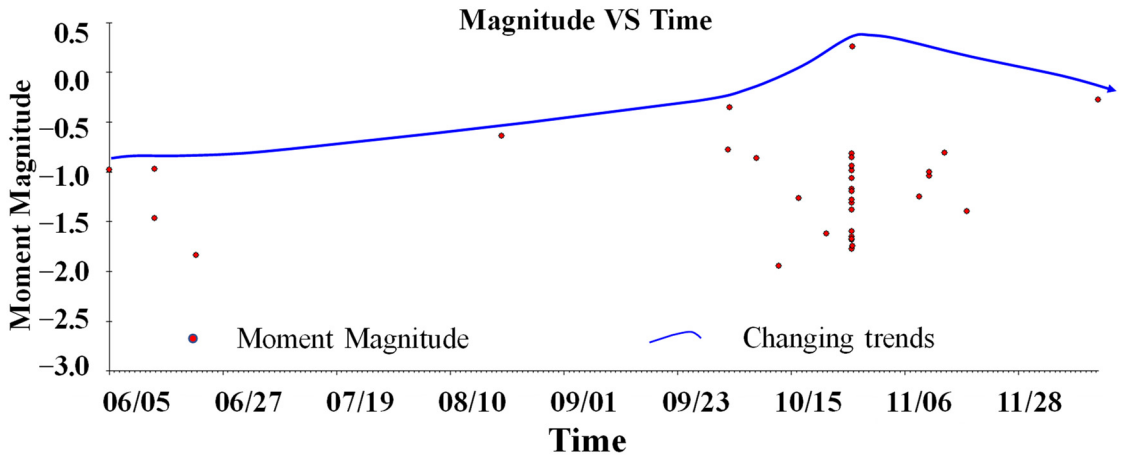

Figure 20. Spatial concentration relationship diagram of underground microseismic positioning events in 2018.

4. Discussion and Conclusions

On 28 June 2013, a large-scale roof collapse and ground pressure display event occurred at the four pits where the eastern and western mining areas of Xianglushan Tungsten Mine intersect. The collapse of the large-scale mined-out area caused the stress transfer and redistribution of the whole mine and triggered ground pressure manifestation events of different scales in many regions. Through certain monitoring methods such as microseismic monitoring we can reproduce the change process of ground pressure and stress transfer before and after the event, to analyze its internal characteristics, summarize the change rules, and finally, provide response references for similar mines and accidents. Specifically, we discussed the characteristics of microseismic event concentration in different working conditions and different locations, for example, the distribution of ground pressure transfer and microseismic events in a strip pattern, and the distribution of the main top concentrated areas. In addition, the data on surface subsidence, energy release, and ore yield were verified. In general, the data conform to the overall trend of ground pressure distribution and the actual objective working conditions of the mine site.

Taking Xianglushan Tungsten Mine as the engineering background, the microseismic monitoring system was built to analyze the ground pressure manifestation law, and the ground pressure transfer characteristics were comprehensively analyzed in combination with microseismic events and residual mining. The ground pressure transfer and distribution were analyzed from different spatial angles, and the ground pressure manifestation characteristics in different periods before and after were compared on the timeline. Finally, the system was verified and analyzed by auxiliary parameters such as ore yield, surface subsidence, and energy release. The main conclusions are as follows:

(1) For the complete hard rock, when its stress increases, there will be micro-shock/acoustic emission, which is the direct manifestation of the internal micro-fracture of the rock, until the occurrence of macro-cracks, rock mass failure and instability, roof caving, pillar spalling, pillar burst, and other macro-ground pressure phenomena such as the occurrence of micro-shock signals will inevitably increase.

(2) The temporal and spatial distribution characteristics of microseismic positioning events from 2013 to 2018 were summarized and analyzed. The characteristics of microseismic activity reflect the evolution characteristics of the overall ground pressure distribution of the mine, and the relationship between microseismic activity and mining volume and surface subsidence was discussed, to guide mining.

(3) Through the collection of microseismic, stress, and ground pressure data before and after the collapse event of the largest mined-out area in this period, the regional distribution of microseismic activity, stress concentration, and ground pressure mani-

festation were analyzed, and the characteristics of the overall ground pressure of the mine and the changing trend of the overall ground pressure activity were studied. The obtained overall ground pressure law and development trend guide the mining and mined-out area treatment of the mine.

(4) According to the field monitoring data over five years, there are many microseismic events in the year of large-scale collapse events, accounting for 57.4%. Since then, the number of events has decreased significantly, less than 10% of the peak value. The occurrence frequency and intensity of ground pressure tend to ease. In the later stage, the growth rate is relatively fast, which is equivalent to the energy release. The increase in event activity rate is confirmed laterally, reflecting the characteristics of ground pressure transfer and redistribution.

Author Contributions: Methodology, Z.Z. and C.Z.; software, Y.H.; data curation, Y.H.; writing—original draft, Y.H.; writing—review and editing, Z.Z. and C.Z.; supervision, C.Z.; funding acquisition, Z.Z. All authors have read and agreed to the published version of the manuscript.

Funding: This research was funded by the National Natural Science Foundation of China, grant number 52274249, and the National Key Research and Development Program of China, grant number 2022YFC2903901.

Data Availability Statement: The data are available on request, subject to restrictions (e.g., privacy or ethical restrictions).

Acknowledgments: The authors would like to acknowledge the National Natural Science Foundation of China (Project No. 52274249) and the National Key Research and Development Program of China (2022YFC2903901).

Conflicts of Interest: The authors declare no conflict of interest.

References

1. Feng, X.-T.; Young, R.P.; Reyes-Montes, J.M.; Aydan, Ö.; Ishida, T.; Liu, J.-P.; Liu, H.-J. ISRM Suggested Method for In Situ Acoustic Emission Monitoring of the Fracturing Process in Rock Masses. *Rock Mech. Rock Eng.* **2019**, *52*, 1395–1414. [CrossRef]
2. Bi, Y.; Wang, M.; Wu, C.; Huang, Y. Surrounding Rock Stability in Unsupported Roof Area and Rapid Heading Technique for Deep Arch Coal Roadways under Goaf. *Minerals* **2022**, *12*, 1329. [CrossRef]
3. Cai, X.; Zhou, Z.; Tan, L.; Zang, H.; Song, Z. Water Saturation Effects on Thermal Infrared Radiation Features of Rock Materials During Deformation and Fracturing. *Rock Mech. Rock Eng.* **2020**, *53*, 4839–4856. [CrossRef]
4. Cai, W.; Chang, Z.; Zhang, D.; Wang, X.; Cao, W.; Zhou, Y. Roof filling control technology and application to mine roadway damage in small pit goaf. *Int. J. Min. Sci. Technol.* **2019**, *29*, 477–482. [CrossRef]
5. Ma, D.; Duan, H.; Liu, J.; Li, X.; Zhou, Z. The role of gangue on the mitigation of mining-induced hazards and environmental pollution: An experimental investigation. *Sci. Total Environ.* **2019**, *664*, 436–448. [CrossRef]
6. Liu, Y.; Wen, H.; Guo, J.; Jin, Y.; Wei, G.; Yang, Z. Coal spontaneous combustion and N-2 suppression in triple goaves: A numerical simulation and experimental study. *Fuel* **2020**, *271*, 117625. [CrossRef]
7. Mu, W.; Li, L.; Zhang, Y.; Yu, G.; Ren, B. Failure Mechanism of Grouted Floor with Confined Aquifer Based on Mining-Induced Data. *Rock Mech. Rock Eng.* **2023**, *56*, 1–26. [CrossRef]
8. Khan, S.; Khulief, Y.A.; Al-Shuhail, A.A. Effects of reservoir size and boundary conditions on pore-pressure buildup and fault reactivation during CO_2 injection in deep geological reservoirs. *Environ. Earth Sci.* **2020**, *79*, 1–23. [CrossRef]
9. Zhou, Z.; Chen, L.; Cai, X.; Shen, B.; Zhou, J.; Du, K. Experimental Investigation of the Progressive Failure of Multiple Pillar-Roof System. *Rock Mech. Rock Eng.* **2018**, *51*, 1629–1636. [CrossRef]
10. Zhou, Z.; Zang, H.; Cao, W.; Du, X.; Chen, L.; Ke, C. Risk assessment for the cascading failure of underground pillar sections considering the interaction between pillars. *Int. J. Rock Mech. Min. Sci.* **2019**, *124*, 104142. [CrossRef]
11. Zhou, Z.; Zhao, Y.; Cao, W.; Chen, L.; Zhou, J. Dynamic Response of Pillar Workings Induced by Sudden Pillar Recovery. *Rock Mech. Rock Eng.* **2018**, *51*, 3075–3090. [CrossRef]
12. Turquet, A.L.; Toussaint, R.; Eriksen, F.K.; Daniel, G.; Koehn, D.; Flekkoy, E.G. Microseismic Emissions During Pneumatic Fracturing: A Numerical Model to Explain the Experiments. *J. Geophys. Res.-Solid Earth* **2018**, *123*, 6922–6939. [CrossRef]
13. Arosio, D.; Longoni, L.; Papini, M.; Boccolari, M.; Zanzi, L. Analysis of microseismic signals collected on an unstable rock face in the Italian Prealps. *Geophys. J. Int.* **2018**, *213*, 475–488. [CrossRef]
14. Li, P.X.; Chen, B.-R.; Xiao, Y.-X.; Feng, G.-L.; Zhou, Y.-Y.; Zhao, J.-S. Rockburst and microseismic activity in a lagging tunnel as the spacing between twin TBM excavated tunnels changes: A case from the Neelum-Jhelum hydropower project. *Tunn. Undergr. Space Technol.* **2023**, *132*, 104884. [CrossRef]
15. Colombero, C.; Comina, C.; Vinciguerra, S.; Benson, P.M. Microseismicity of an Unstable Rock Mass: From Field Monitoring to Laboratory Testing. *J. Geophys. Res.-Solid Earth* **2018**, *123*, 1673–1693. [CrossRef]

16. Kang, H.; Jiang, P.; Feng, Y.; Gao, F.; Zhang, Z.; Liu, X. Application of Large-Scale Hydraulic Fracturing for Reducing Mining-Induced Stress and Microseismic Events: A Comprehensive Case Study. *Rock Mech. Rock Eng.* **2022**, *56*, 1399–1413. [CrossRef]
17. Ma, K.; Wang, H.; Liao, Z.; Peng, Y.; Wang, K. Precursor of microseismic energy and stress evolution induced by rockburst in coal mining: A case study from Xiashijie, Shannxi, China. *Geomech. Geophys. Geo-Energy Geo-Resour.* **2022**, *8*, 134. [CrossRef]
18. Liu, J.-P.; Si, Y.-T.; Wei, D.-C.; Shi, H.-X.; Wang, R. Developments and prospects of microseismic monitoring technology in underground metal mines in China. *J. Cent. South Univ.* **2021**, *28*, 3074–3098. [CrossRef]
19. Zimmermann, G.; Zang, A.; Stephansson, O.; Klee, G.; Semikova, H. Permeability Enhancement and Fracture Development of Hydraulic In Situ Experiments in the Aspo Hard Rock Laboratory, Sweden. *Rock Mech. Rock Eng.* **2019**, *52*, 495–515. [CrossRef]
20. Contrucci, I.; Balland, C.; Kinscher, J.; Bennani, M.; Bigarre, P.; Bernard, P. Aseismic Mining Subsidence in an Abandoned Mine: Influence Factors and Consequences for Post-Mining Risk Management. *Pure Appl. Geophys.* **2019**, *176*, 801–825. [CrossRef]
21. Baird, A.F.; Stork, A.L.; Horne, S.A.; Naldrett, G.; Kendall, J.M.; Wookey, J.; Verdon, J.P.; Clarke, A. Characteristics of microseismic data recorded by distributed acoustic sensing systems in anisotropic media. *Geophysics* **2020**, *85*, KS139–KS147. [CrossRef]
22. Hamid, M. Coal pillar mechanics of violent failure in U.S. Mines. *Int. J. Min. Sci. Technol.* **2017**, *27*, 387–392.
23. Andersson, J.C.; Martin, C.D. The Aspo pillar stability experiment: Part I-Experiment design. *Int. J. Rock Mech. Min. Sci.* **2009**, *46*, 865–878. [CrossRef]
24. Das, A.J.; Mandal, P.K.; Bhattacharjee, R.; Tiwari, S.; Kushwaha, A.; Roy, L.B. Evaluate notion of stability of underground workings for exploitation of an inclined coal seam by the ubiquitous joint model. *Int. J. Rock Mech. Min. Sci.* **2017**, *93*, 101–114. [CrossRef]
25. Liu, Q.-S.; Wu, J.; Zhang, X.-P.; Tang, L.-X.; Bi, C.; Li, W.-W.; Xu, J.-L. Microseismic Monitoring to Characterize Structure-Type Rockbursts: A Case Study of a TBM-Excavated Tunnel. *Rock Mech. Rock Eng.* **2020**, *53*, 2995–3013. [CrossRef]
26. Ma, K.; Sun, X.Y.; Tang, C.A.; Yuan, F.Z.; Wang, S.J.; Chen, T. Floor water inrush analysis based on mechanical failure characters and microseismic monitoring. *Tunn. Undergr. Space Technol.* **2021**, *108*, 103698. [CrossRef]
27. Zuo, J.; Wu, G.; Du, J.; Lei, B.; Li, Y. Rock Strata Failure Behavior of Deep Ordovician Limestone Aquifer and Multi-level Control Technology of Water Inrush Based on Microseismic Monitoring and Numerical Methods. *Rock Mech. Rock Eng.* **2022**, *55*, 4591–4614. [CrossRef]
28. D'Angio, D.; Lenti, L.; Martino, S. Microseismic monitoring to assess rock mass damaging through a novel damping ratio-based approach. *Int. J. Rock Mech. Min. Sci.* **2021**, *146*, 104883. [CrossRef]
29. Liu, J.-P.; Wang, R.; Lei, G.; Si, Y.-T.; Xu, S.-D.; Li, Y.-H. Studies of stress and displacement distribution and the evolution law during rock failure process based on acoustic emission and microseismic monitoring. *Int. J. Rock Mech. Min. Sci.* **2020**, *132*, 104384. [CrossRef]
30. Zhang, S.; Ma, T.; Tang, C.A.; Jia, P.; Wang, Y. Microseismic Monitoring and Experimental Study on Mechanism of Delayed Rockburst in Deep-Buried Tunnels. *Rock Mech. Rock Eng.* **2020**, *53*, 2771–2788. [CrossRef]
31. Zhao, Y.; Yang, T.; Liu, H.; Wang, S.; Zhang, P.; Jia, P.; Wang, X. A path for evaluating the mechanical response of rock masses based on deep mining-induced microseismic data: A case study. *Tunn. Undergr. Space Technol.* **2021**, *115*, 104025. [CrossRef]
32. Zhao, Y.; Yang, T.; Zhang, P.; Xu, H.; Zhou, J.; Yu, Q. Method for Generating a Discrete Fracture Network from Microseismic Data and its Application in Analyzing the Permeability of Rock Masses: A Case Study. *Rock Mech. Rock Eng.* **2019**, *52*, 3133–3155. [CrossRef]
33. Li, A.; Dai, F.; Xu, N.; Gu, G.; Hu, Z. Analysis of a Complex Flexural Toppling Failure of Large Underground Caverns in Layered Rock Masses. *Rock Mech. Rock Eng.* **2019**, *52*, 3157–3181. [CrossRef]
34. Niemz, P.; Dahm, T.; Milkereit, C.; Cesca, S.; Petersen, G.; Zang, A. Insights into Hydraulic Fracture Growth Gained from a Joint Analysis of Seismometer-Derived Tilt Signals and Acoustic Emissions. *J. Geophys. Res.-Solid Earth* **2021**, *126*, e2021JB023057. [CrossRef]
35. Wu, Y.; Shi, Y.; Dai, R.; Ji, H.; Yang, X.; Zhang, D.; Chang, Y. Ground Pressure Risk Early Warning Method, Involves Performing Spatio-Temporal Trend Analysis on Multiple Source Parameters and Characteristic Parameters of Microseismic Events in Potential Risk Concern Area to Determine Land Pressure Risk Area and Risk Level. Chinese Patent CN115343757-A, 15 November 2022.
36. Ma, T.-H.; Tang, C.-A.; Tang, S.-B.; Kuang, L.; Yu, Q.; Kong, D.-Q.; Zhu, X. Rockburst mechanism and prediction based on microseismic monitoring. *Int. J. Rock Mech. Min. Sci.* **2018**, *110*, 177–188. [CrossRef]
37. Stolecki, L.; Grzebyk, W. The velocity of roof deflection as an indicator of underground workings stability-Case study from polish deep copper mines. *Int. J. Rock Mech. Min. Sci.* **2021**, *143*, 104717. [CrossRef]
38. Zhang, Y.; Ni, P. Design optimization of room and pillar mines: A case study of the Xianglushan tungsten mine. *Q. J. Eng. Geol. Hydrogeol.* **2018**, *51*, 352–364. [CrossRef]
39. Jiao, H.; Yang, W.; Shen, H.; Yang, Y.; Liu, J. Study on Multi-Layer Filling Treatment of Extra-Large Goaf and Its Underground Application. *Materials* **2022**, *15*, 5680. [CrossRef]
40. Liu, L.; Zhou, P.; Feng, Y.; Zhang, B.; Song, K.-I. Quantitative investigation on micro-parameters of cemented paste backfill and its sensitivity analysis. *J. Cent. South Univ.* **2020**, *27*, 267–276. [CrossRef]
41. Liu, Y.-c.; Li, S.-l.; Tang, C. Improvement and application of focal mechanism solution type criterion for rock mass fracture. *Rock Soil Mech.* **2021**, *42*, 1335.
42. Liu, L.; Xin, J.; Qi, C.; Jia, H.; Song, K.-I. Experimental investigation of mechanical, hydration, microstructure and electrical properties of cemented paste backfill. *Constr. Build. Mater.* **2020**, *263*, 120137. [CrossRef]

43. Liu, L.; Xin, J.; Feng, Y.; Zhang, B.; Song, K.I.I. Effect of the Cement-Tailing Ratio on the Hydration Products and Microstructure Characteristics of Cemented Paste Backfill. *Arab. J. Sci. Eng.* **2019**, *44*, 6547–6556. [CrossRef]
44. Zhao, Y.; Zhao, G.; Xu, L.; Zhou, J.; Huang, X. Mechanical property evolution model of cemented tailings-rock backfill considering strengthening and weakening effects. *Constr. Build. Mater.* **2023**, *377*, 131081. [CrossRef]
45. Gu, H.; Lai, X.; Tao, M.; Cao, W.; Yang, Z. The role of porosity in the dynamic disturbance resistance of water-saturated coal. *Int. J. Rock Mech. Min. Sci.* **2023**, *16*, 105388. [CrossRef]